JACS
JOURNAL OF THE AMERICAN CHEMICAL SOCIETY

Communication

pubs.acs.org/JACS

Planar Heterojunction Perovskite Solar Cells via Vapor-Assisted Solution Process

Qi Chen,[†,‡,+] Huanping Zhou,*[,†,‡,+] Ziruo Hong,[†] Song Luo,[†,‡] Hsin-Sheng Duan,[†,‡] Hsin-Hua Wang,[†,‡] Yongsheng Liu,[†,‡] Gang Li,[†,‡] and Yang Yang*[,†,‡]

[†]Department of Materials Science and Engineering and [‡]California NanoSystems Institute, University of California, Los Angeles, California 90095, United States

Supporting Information

ABSTRACT: Hybrid organic/inorganic perovskites (e.g., $CH_3NH_3PbI_3$) as light absorbers are promising players in the field of third-generation photovoltaics. Here we demonstrate a low-temperature vapor-assisted solution process to construct polycrystalline perovskite thin films with full surface coverage, small surface roughness, and grain size up to microscale. Solar cells based on the as-prepared films achieve high power conversion efficiency of 12.1%, so far the highest efficiency based on $CH_3NH_3PbI_3$ with the planar heterojunction configuration. This method provides a simple approach to perovskite film preparation and paves the way for high reproducibility of films and devices. The underlying kinetic and thermodynamic parameters regarding the perovskite film growth are discussed as well.

Hybrid organic/inorganic perovskite materials (e.g., $CH_3NH_3PbI_3$) are currently among the most competitive candidates for absorber materials for thin-film photovoltaic (PV) applications.[1] Within the past 4 years, perovskite solar cells have been reported to achieve remarkably high efficiency of ~15%.[2] The reason for this rapid increase in power conversion efficiency (PCE) of such devices is that perovskite materials possess most of the properties required to be excellent absorbers: appropriate direct bandgap, high absorption coefficient, excellent carrier transport, and apparent tolerance of defects.[1b] Besides their extremely low cost and ease of fabrication, perovskite materials offer a wide tunability on composition and structure by adjusting the metal halide framework and the intercalated organic species. Pioneering work suggested that these perovskite films exhibit composition-/structure-dependent properties, which can be accessed by various processing approaches.[3] It is essential to achieve fine control over the reaction between the inorganic and organic species, resulting in perovskites with desired properties and device performance.

Although first implemented in dye-sensitized solar cells based on mesoporous structures,[4] the perovskites have been gradually found to assume all of the principal roles of PV operation,[5] and PV devices with planar architecture have been demonstrated.[2b,6] Planar architecture potentially provides enhanced flexibility for device optimization, multijunction construction, and investigation of the underlying device physics, but it requires tremendous effort to fabricate high-quality perovskite films. Similar to other thin-film PV technologies (e.g., α-Si, $Cu(InGa)S_2$, and CdTe), vacuum evaporation is one of the most promising techniques to construct perovskite thin films for planar junctions. The resulting perovskites prepared by co-evaporation of two precursors ($PbCl_2$ and CH_3NH_3I) exhibit satisfactory film coverage and uniformity within expectations.[2b] However, this technique demands high vacuum, which is too energy consuming and hinders mass production. Alternatively, solution-based techniques have also been proposed to fabricate thin films, in which a mixture of two precursors is used to form the completed absorber. Due to the lack of suitable solvents that can dissolve both components, and the high reaction rate of the perovskite component, this process often results in thin films with pinhole formation and incomplete surface coverage, which deteriorates the film quality and hampers the device performance.[6a] As a variation to this method, a two-step approach was demonstrated to fabricate efficient PV devices by dipping previously deposited inorganic precursor films into solutions containing organic species.[2a] Unfortunately, this method has been largely successful in films with nanostructured TiO_2 scaffolds[2a] but is seldom reported to be applicable for fabricating planar heterojunctions. Constructing a $CH_3NH_3PbI_3$ film with a thickness of several hundred nanometers requires long reaction times due to the limited reaction interface area. The two-step process also often results in films with strikingly enhanced surface roughness that frequently peel off from the substrate.[7] As such, there is an urge to develop a facile solution approach to perovskite materials with enhanced controllability of the film quality to construct planar structured devices with competitive performance.

Scheme 1. Schematic Illustration of Perovskite Film Formation through Vapor-Assisted Solution Process

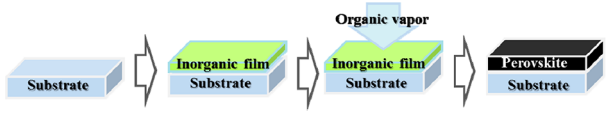

In this Communication, we demonstrate use of the vapor-assisted solution process (VASP) to fabricate perovskite thin films and subsequently PV devices with planar geometry. The key step is film growth via in situ reaction of the as-deposited film of PbI_2 with CH_3NH_3I vapor (Scheme 1). This method is conceptually different from the current solution process and vacuum deposition, by avoiding co-deposition of organic and

Received: November 12, 2013
Published: December 20, 2013

   dx.doi.org/10.1021/ja411509g | J. Am. Chem. Soc. 2014, 136, 622−625

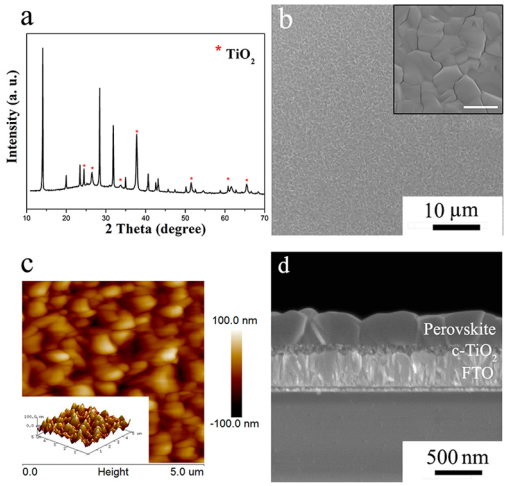

Figure 1. Perovskite film on the FTO/c-TiO_2 substrate, obtained by reacting PbI_2 film and CH_3NH_3I vapor at 150 °C for 2 h in N_2 atmosphere: (a) XRD pattern; (b) top-view SEM image (inset image with higher resolution, scale bar 1 μm); (c) tapping-mode AFM height images (5 × 5 μm) (inset: the corresponding 3D topographic image); and (d) cross-sectional SEM image.

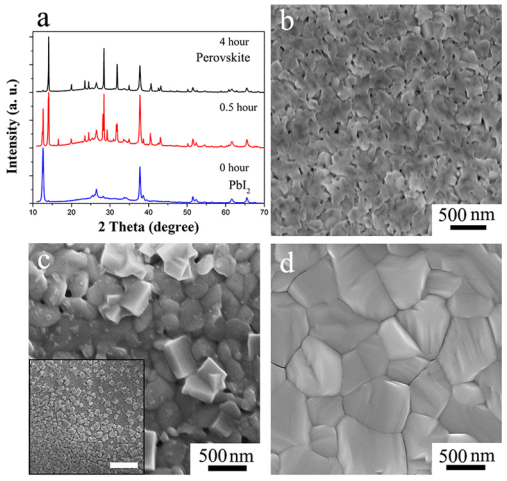

Figure 2. Time evolution characterization of the perovskite thin film by annealing ~200 nm PbI_2 film in the presence of CH_3NH_3I at 150 °C in N_2 atmosphere: (a) XRD patterns of the film annealed at 0, 0.5, and 4 h; (b–d) top-view SEM images of (b) the initial stage at 0 h, (c) the intermediate stage at 0.5 h (inset: wider view, scale bar 3 μm), and (d) the post stage at 4 h.

inorganic species. It takes advantage of the kinetic reactivity of CH_3NH_3I and thermodynamic stability of perovskite during the in situ growth process and provides films with well-defined grain structure with grain sizes up to microscale, full surface coverage, and small surface roughness, suitable for PV applications. Devices based on films prepared via VASP achieved a best PCE of 12.1%, so far the highest efficiency of $CH_3NH_3PbI_3$ with planar structure.

VASP was developed to fabricate organic/inorganic hybrid perovskite film (e.g., $CH_3NH_3PbX_3$, X = Cl, Br, I), where the inorganic framework film is formed by depositing precursor solution on the substrates and subsequently treated with the desired organic vapor (Scheme 1). As an illustration, PbI_2 and CH_3NH_3I are the corresponding precursor couple to form $CH_3NH_3PbI_3$ in this work (see the Supporting Information (SI) for details). PbI_2 films were deposited on fluorine-doped tin oxide (FTO) glass coated with a compact layer of TiO_2 (c-TiO_2), followed by annealing in CH_3NH_3I vapor at 150 °C in N_2 atmosphere for 2 h to form the perovskite films. Figure 1a shows the corresponding X-ray diffraction (XRD) of the as-prepared $CH_3NH_3PbI_3$ film on FTO/c-TiO_2 substrate. A set of strong peaks at 14.08°, 28.41°, 31.85°, and 43.19°, assigned to (110), (220), (310), and (330) of the $CH_3NH_3PbI_3$ crystal,[4a,8] indicate an orthorhombic crystal structure of halide perovskite with high crystallinity. According to the literature,[2b] there is often a tiny signature peak at 12.65°, corresponding to a low-level impurity of PbI_2. The absence of the aforementioned peak in the present perovskite film suggests complete consumption of PbI_2 via VASP. The film quality of the perovskite is further evaluated by scanning electron microscopy (SEM) and atomic force microscopy (AFM). As shown in Figure 1b, the as-formed perovskite film possesses the characteristics of full surface coverage on the substrates, with remarkable grain size up to microscale. The surface roughness of the film was measured by AFM (Figure 1c) and calculated to be 23.2 nm in the range of 5 μm × 5 μm. The roughness of the film fabricated via VASP is relatively small compared to other solution processed films,[7] regardless of its microscale grain size. A typical cross-sectional SEM image indicates the resulting film has a thickness of ~350 nm, with well-defined grains across the film thickness. The 100% surface coverage, microscale grain size, and uniform grain structure of the as-prepared film suggest its promising applicability for PV devices. These overwhelming characteristics could be due to the combination of the relative smoothness of the preformed PbI_2 film, the effective intercalation of CH_3NH_3I vapor into the inorganic framework, as will be discussed later.

Film formation is crucial to fabricate planar heterojunctions in most thin-film PV techniques; it is thus necessary to understand the underlying kinetic and thermodynamic mechanism of perovskite thin-film fabrication via VASP. Perovskite thin-film evolution was investigated by annealing ~200 nm thick PbI_2 films in the presence of CH_3NH_3I at 150 °C in N_2 atmosphere for different lengths of time. Four representative samples with different annealing times were prepared: the initial stage (0 h, Figure 2b), intermediate stage (0.5 h, Figure 2c), complete stage (2 h, Figure 1b), and post stage (4 h, Figure 2d). (SEM images of samples of 1 and 3 h are included in Figure S2.) The XRD pattern (Figure 2a) clearly shows that, at the initial stage, the film is composed of PbI_2 phase, while in the intermediate stage, both phases, PbI_2 and perovskite, coexist in the film as evidenced by the appearance of their corresponding peaks. With time evolution, the PbI_2 phase disappears at the complete stage, and no new peak is observed at the post stage.

The grain structure of the corresponding deposited film changes strikingly along with the intercalation reaction as well. The initial PbI_2 film exhibits uniform polygon grains of a few hundred nanometers, as well as scattered voids among adjacent grains. As the PbI_2 film was exposed to CH_3NH_3I vapor for 30 min, it exhibited two distinct shapes with different contrast. The dark grains show morphology similar to those in Figure 2b, considered to be unreacted PbI_2. The relatively light grains appeared right on the top of the original PbI_2 film with larger grain size and different grain morphology. As the coexistence of two phases in the film is confirmed by the XRD pattern, they are speculated to be the newly formed perovskite. These species on the top of PbI_2 films significantly promote the film thickening, as shown in Figure S1b, probably due to volume expansion from intercalation of CH_3NH_3I, accompanied by transformation of the

dx.doi.org/10.1021/ja411509g | J. Am. Chem. Soc. 2014, 136, 622–625

PbI_2 framework from the originally edge-sharing octahedral structure to the corner-sharing octahedral structure in perovskite films.[8a] Note the appearance of some dots with sizes of tens of nanometers on the surface of unreacted PbI_2. It is highly suspected that these tiny dots are reactive "nuclei" for the growth of grains, originating from the reaction between PbI_2 and CH_3NH_3I vapor. With the presence of the newly formed perovskite crystals on top, along with the "nuclei" decorated around, we believe that the intercalation reaction takes place on top of the PbI_2 film in this stage. As the reaction time increases to 2 h, perovskite films with grain size up to the microscale are observed. Compared to the original PbI_2 film, the perovskite film differs in both morphology and size, where the film thickness of perovskite increases to ~350 nm from the original PbI_2 film of ~200 nm (Figure S1a). The in-plane grain size of perovskite is 3 times the film thickness, indicating that the growth of perovskite polycrystalline films follows normal grain growth mode.[9] In addition, the voids present in between the adjacent crystals in the original PbI_2 film vanished after the perovskite crystals formed. Interestingly, further prolonging the reaction time to 4 h does not affect the grain structure (Figure 2d). There is no obvious ripening, or coarsening process at post stage, which often appears during polycrystalline film growth,[10] indicating that a thermodynamically stable film is formed after the reaction is complete at the moderate temperature. Further prolonging the reaction time is outside of the current research scope, though.

The present VASP results in perovskite films with full surface coverage, small surface roughness, and complete conversion of PbI_2, addressing most crucial issues regarding perovskite thin-film formation for PV applications. Remarkably different from previously reported solution processing approaches, the two-step VASP exhibits its distinctiveness. In the first step, the inorganic precursors are deposited to form a smooth and uniform PbI_2 film with a surface roughness of <20 nm (Figure S3). It avoids the extremely high reaction rate of perovskite film often observed in the co-deposition process.[7] This film acts not only as a superior framework for the perovskite formation but also as a reservoir for one of the reactants to provide the kinetically favorable "nucleation" centers for further perovskite formation. Upon exposure to the CH_3NH_3I vapor in the second step, the intercalation reaction occurs in situ with simultaneous polycrystalline film growth, where the specific surface and interface-energy-minimizing crystallographic orientations are favored. The enhanced grain size can be ascribed to volume expansion during the transformation from PbI_2 to perovskite by the intercalation of CH_3NH_3I, as well as rearrangement of the aggregated structure of PbI_2 driven by the reduction of boundary length to minimize the grain boundary energy.[10] The absence of voids in the final film, in contrast to the original PbI_2 film, suggests that VASP promotes a rearrangement of PbI_2 and/or reorganization of PbI_2 and CH_3NH_3I via intensive diffusion during film growth.[11] Note that VASP is especially applicable in fabricating the 3D structure thin films compared to the conventional two-step solution process. Since there is no kinetically favorable van der Waals gap in the $PbI_2/CH_3NH_3PbI_3$ interface where the transformation can occur,[7,12] a rather long reaction time is required to transform inorganic precursors into perovskite completely. Films often deteriorated upon extended dipping. In VASP, however, the absence of solvent media and a moderate processing temperature collectively contribute a complete reaction between PbI_2 and CH_3NH_3I without impairing the film quality.

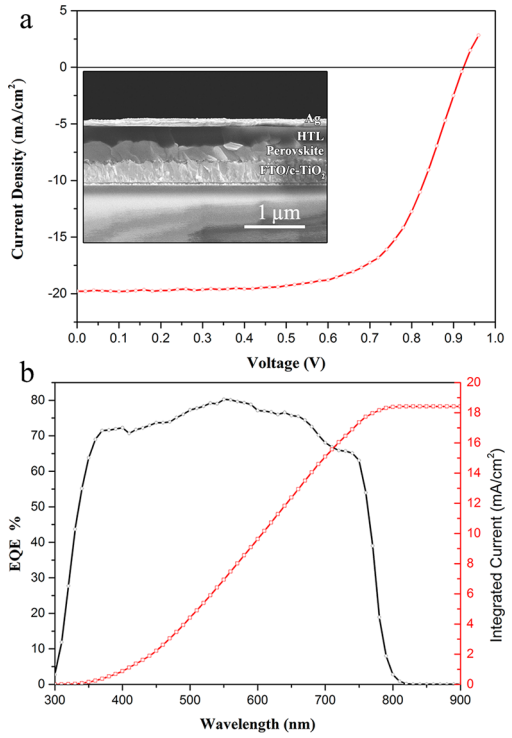

Figure 3. (a) Current density–voltage (J–V) characteristics of the solar cell based on the as-prepared perovskite films under AM 1.5G illumination, and cross-sectional SEM image of the device (inset). (b) EQE spectrum (black) and the integrated photocurrent (red) expected to be generated under AM 1.5G irradiation of the device.

The as-formed perovskite films with complete conversion of PbI_2, after a proper postannealing time, were subsequently used for PV device fabrication. The detailed device fabrication process is described in the SI. The cross-sectional SEM image of the device reveals its planar architecture, where the absorber layer is well implemented into the device with intimate contact to adjacent layers: the FTO substrate is coated with a compact layer of TiO_2 (~70 nm), followed by the $CH_3NH_3PbI_3$ layer (~350 nm). 2,2′,7,7′-Tetrakis(*N*,*N*-di-*p*-methoxyphenylamine)-9,9′-spirobifluorene with a thickness of ~300 nm is employed as a hole-transporting layer. A thermally evaporated silver layer (~100 nm) forms the back contact of the device.

The corresponding device performance is characterized by current density (J)–voltage (V) measurement under simulated AM 1.5G (100 mW/cm^2) solar irradiation in the air. As shown in Figure 3a, the optimum device exhibits outstanding performance, with J_{SC} = 19.8 mA/cm^2, V_{OC} = 0.924 V, fill factor (FF) = 66.3%, and PCE = 12.1%, so far the highest efficiency based on $CH_3NH_3PbI_3$ with planar structure. In general, the devices exhibit V_{OC} = 0.83–0.94 V, J_{SC} = 17.3–20.8 mA/cm^2, FF = 56.0–68.2%, and the resulting PCE = 9.3–12.1%. Figure 3b shows the external quantum efficiency (EQE) spectrum for the perovskite cell. Photocurrent generation starts at 780 nm, in agreement with the bandgap of the $CH_3NH_3PbI_3$,[4c] and reaches peak values of ~80% in the visible spectrum. Integrating the overlap of the EQE spectrum with the AM 1.5G solar photon flux yields a current density of 18.5 mA/cm^2. The slightly lower current density obtained from EQE measurement, compared to that from the J–V curve, can probably be attributed to the surface trap of the TiO_2 transporting layer.[13] An important factor contributing to the high PCE is the high quality of the absorber film fabricated via VASP. The full surface coverage of this film provides more absorption to

dx.doi.org/10.1021/ja411509g | *J. Am. Chem. Soc.* 2014, 136, 622–625

contribute to the high J_{SC}. The large grains with reduced grain boundaries, and the uniform nature in the vertical direction over a range of length scale, may help to alleviate surface recombination when carriers are transported in the perovskite layer, leading to high V_{OC}. The improvement of FF is largely attributed to the decrease of parasitic loss currents and the parallel resistance of the devices in this pinhole-free thin film. Note that the reported minority carrier diffusion length for $CH_3NH_3PbI_3$ is quite short, ~100 nm, resulting in relatively low device efficiencies (normally <10%) within the planar device architecture.[5a,b] The remarkably high efficiency of 12.1% based on present $CH_3NH_3PbI_3$ may result from the improved electrical property of the high-quality film. Further study toward understanding of the relevance between the film property and device performance is underway.

In summary, we report VASP, a novel low-temperature approach to fabricate planar perovskite films and their corresponding PV devices, based on the kinetically favorable reaction between the as-deposited film of PbI_2 and CH_3NH_3I vapor. The perovskite film derived from this approach exhibits full surface coverage, uniform grain structure with grain size up to micrometers, and 100% precursor transformation completeness. A film evolution study on perovskite transformation indicates an appropriate rearrangement of PbI_2 film during intercalation of CH_3NH_3I driven by the reduction of grain boundary energy. Facilitated by the excellent film quality, the $CH_3NH_3PbI_3$ materials enable an impressive device PCE of 12.1% in a planar architecture. VASP presents a simple, controllable, and versatile approach to the pursuit of high-quality perovskite film and the resulting high-performance PV devices. Incorporating organic species into the as-deposited inorganic framework through vapor effectively avoids the high reaction rate of perovskite during co-deposition of precursors and concern about possible film deterioration when dipping an inorganic framework into an organic species solution. Future work will focus on property investigation within the resulting films, e.g., charge transport behavior. More importantly, continuous advancement of film engineering will enable high-performance perovskite solar cells and other organic/inorganic hybrid optoelectronics. The fabrication of other optoelectronics, e.g., light-emitting diodes, field effect transistors, and detectors, may also benefit from VASP.

■ ASSOCIATED CONTENT

Supporting Information

Experimental details and Figures S1−S5. This material is available free of charge via the Internet at http://pubs.acs.org.

■ AUTHOR INFORMATION

Corresponding Authors

happyzhou@ucla.edu
yangy@ucla.edu

Author Contributions

[+]Q.C. and H.Z. contributed equally to this work.

Notes

The authors declare no competing financial interest.

■ ACKNOWLEDGMENTS

This work was financially supported by a grant from the National Science Foundation (grant no. ECCS-1202231, Program Director Dr. George N. Maracas), Air Force Office of Scientific Research (grant no. FA9550-12-1-0074, Program Manager Dr. Charles Lee), and UCLA Internal Funds. The authors sincerely acknowledge Prof. King-Ning Tu of UCLA and Dr. Su-Huai Wei of NREL for valuable discussion on the crystal growth mechanism and the band structure of the perovskite crystal. Also, we acknowledge Dr. Xiaolei Wang, Dr. Ge Li, and Eric Richard for their help on the electrode fabrication, the graphic drawing, and English editing.

■ REFERENCES

(1) (a) Park, N.-G. *J. Phys. Chem. Lett.* **2013**, *4*, 2423. (b) Snaith, H. J. *J. Phys. Chem. Lett.* **2013**, *4*, 3623.

(2) (a) Burschka, J.; Pellet, N.; Moon, S.-J.; Humphry-Baker, R.; Gao, P.; Nazeeruddin, M. K.; Gratzel, M. *Nature* **2013**, *499*, 316. (b) Liu, M.; Johnston, M. B.; Snaith, H. J. *Nature* **2013**, *501*, 395.

(3) (a) Kagan, C.; Mitzi, D.; Dimitrakopoulos, C. *Science* **1999**, *286*, 945. (b) Mitzi, D. B. *Prog. Inorg. Chem.* **2007**, *48*, 1.

(4) (a) Im, J.-H.; Lee, C.-R.; Lee, J.-W.; Park, S.-W.; Park, N.-G. *Nanoscale* **2011**, *3*, 4088. (b) Kojima, A.; Teshima, K.; Shirai, Y.; Miyasaka, T. *J. Am. Chem. Soc.* **2009**, *131*, 6050. (c) Kim, H. S.; Lee, C. R.; Im, J. H.; Lee, K. B.; Moehl, T.; Marchioro, A.; Moon, S. J.; Humphry-Baker, R.; Yum, J. H.; Moser, J. E.; Gratzel, M.; Park, N. G. *Sci. Rep.* **2012**, *2*, 591. (d) Lee, M. M.; Teuscher, J.; Miyasaka, T.; Murakami, T. N.; Snaith, H. J. *Science* **2012**, *338*, 643. (e) Heo, J. H.; Im, S. H.; Noh, J. H.; Mandal, T. N.; Lim, C.-S.; Chang, J. A.; Lee, Y. H.; Kim, H.-j.; Sarkar, A.; Nazeeruddin, Md. K.; Gratzel, M.; Seok, S. I. *Nat. Photon.* **2013**, *7*, 486. (f) Abrusci, A.; Stranks, S. D.; Docampo, P.; Yip, H.-L.; Jen, A. K. Y.; Snaith, H. J. *Nano Lett.* **2013**, *13*, 3124. (g) Kim, H.-S.; Lee, J.-W.; Yantara, N.; Boix, P. P.; Kulkarni, S. A.; Mhaisalkar, S.; Grätzel, M.; Park, N.-G. *Nano Lett.* **2013**, *13*, 2412. (h) Noh, J. H.; Im, S. H.; Heo, J. H.; Mandal, T. N.; Seok, S. I. *Nano Lett.* **2013**, *13*, 1764. (i) Zhang, W.; Saliba, M.; Stranks, S. D.; Sun, Y.; Shi, X.; Wiesner, U.; Snaith, H. J. *Nano Lett.* **2013**, *13*, 4505.

(5) (a) Stranks, S. D.; Eperon, G. E.; Grancini, G.; Menelaou, C.; Alcocer, M. J. P.; Leijtens, T.; Herz, L. M.; Petrozza, A.; Snaith, H. J. *Science* **2013**, *342*, 341. (b) Xing, G.; Mathews, N.; Sun, S.; Lim, S. S.; Lam, Y. M.; Grätzel, M.; Mhaisalkar, S.; Sum, T. C. *Science* **2013**, *342*, 344. (c) Ball, J. M.; Lee, M. M.; Hey, A.; Snaith, H. J. *Energy Environ. Sci.* **2013**, *6*, 1739. (d) Laban, W. A.; Etgar, L. *Energy Environ. Sci.* **2013**, *6*, 3249. (e) Zhao, Y.; Zhu, K. *J. Phys. Chem. Lett.* **2013**, *4*, 2880. (f) Etgar, L.; Gao, P.; Xue, Z.; Peng, Q.; Chandiran, A. K.; Liu, B.; Nazeeruddin, M. K.; Grätzel, M. *J. Am. Chem. Soc.* **2012**, *134*, 17396. (g) Kim, H.-S.; Mora-Sero, I.; Gonzalez-Pedro, V.; Fabregat-Santiago, F.; Juarez-Perez, E. J.; Park, N.-G.; Bisquert, J. *Nat. Commun.* **2013**, *4*, 2242.

(6) (a) Eperon, G. E.; Burlakov, V. M.; Docampo, P.; Goriely, A.; Snaith, H. J. *Adv. Funct. Mater.* **2013**, DOI: 10.1002/adfm.201302090. (b) Jeng, J.-Y.; Chiang, Y.-F.; Lee, M.-H.; Peng, S.-R.; Guo, T.-F.; Chen, P.; Wen, T.-C. *Adv. Mater.* **2013**, *25*, 3727. (c) Sun, S.; Salim, T.; Mathews, N.; Duchamp, M.; Boothroyd, C.; Xing, G.; Sum, T. C.; Lam, Y.-M. *Energy Environ. Sci.* **2014**, *7*, 399.

(7) Liang, K.; Mitzi, D. B.; Prikas, M. T. *Chem. Mater.* **1998**, *10*, 403.

(8) (a) Baikie, T.; Fang, Y.; Kadro, J. M.; Schreyer, M.; Wei, F.; Mhaisalkar, S. G.; Graetzel, M.; White, T. J. *J. Mater. Chem. A* **2013**, *1*, 5628. (b) Stoumpos, C. C.; Malliakas, C. D.; Kanatzidis, M. G. *Inorg. Chem.* **2013**, *52*, 9019.

(9) Thompson, C. *Annu. Rev. Mater. Sci.* **2000**, *30*, 159.

(10) Ohring, M. *The materials science of thin films*; Academic Press: Boston, 1992.

(11) (a) Era, M.; Hattori, T.; Taira, T.; Tsutsui, T. *Chem. Mater.* **1997**, *9*, 8. (b) Mitzi, D. B.; Prikas, M.; Chondroudis, K. *Chem. Mater.* **1999**, *11*, 542.

(12) Mitzi, D. B.; Dimitrakopoulos, C. D.; Rosner, J.; Medeiros, D. R.; Xu, Z.; Noyan, C. *Adv. Mater.* **2002**, *14*, 1772.

(13) Boschloo, G. K.; Goossens, A. *J. Phys. Chem.* **1996**, *100*, 19489.